



## Special Feature: Automotive Exhaust Catalyst

Research Report

### Selective Catalytic Reduction of NO<sub>x</sub> by Ammonia: Fe/zeolite Catalyst Development and Reaction Analysis

Masaoki Iwasaki

Report received on Dec. 21, 2010

■ **ABSTRACT** ■ Development and characterization of Fe/zeolite, and analysis of the reaction kinetic were conducted to improve the performance for selective catalytic reduction (SCR) of NO<sub>x</sub> by NH<sub>3</sub>. The effects of Fe loading (preparation method and Fe content) and the pore structure and Si/Al<sub>2</sub> ratio of the zeolite species were investigated. Fe/ZSM-5 prepared by chemical vapor deposition (CVD) with high Fe and Al content was the most suitable catalyst with respect to high reactivity and hydrothermal stability. Characterization of the catalyst revealed that three types of Fe species were present. Of these, ion-exchanged Fe were the active sites and were accurately quantified using temperature-programmed desorption (TPD) of NO<sub>2</sub>. For reaction kinetics analyses, adsorption/desorption behavior of NO<sub>2</sub>, elementary SCR kinetics, and the overall reaction mechanism were investigated. At the first stage of NO<sub>2</sub> adsorption, the NO evolution reaction occurred over binuclear Fe sites, and the adsorption strength of NO<sub>2</sub> on the Fe sites was relatively large (138 kJ/mol). The standard SCR reaction was transiently promoted in the absence of gaseous NH<sub>3</sub>, because NH<sub>3</sub> inhibited the rate-determining step. In the fast SCR, however, promotion did not occur, due to the competitive adsorption of NO<sub>2</sub> and NH<sub>3</sub>. Analysis of the overall reaction presented a general scheme for the SCR mechanism, including the rate-determining step, and common reactions via three SCR and a low-temperature route for NO<sub>2</sub> SCR.

■ **KEYWORDS** ■ Catalyst, Nitrogen oxide, SCR, Iron, Zeolite, Ammonia, Reaction mechanism

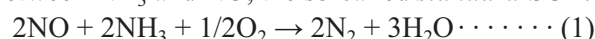
#### 1. Introduction

Nitrogen oxides NO<sub>x</sub> (NO + NO<sub>2</sub>) emitted from mobile and stationary sources are a major source of acid rain and photochemical smog, and they have a directly harmful effect on human health. The limits for NO<sub>x</sub> emissions from mobile vehicles have become more restrictive in recent years.<sup>(1)</sup> Selective catalytic reduction (SCR) by ammonia is one of the most efficient technologies used for the removal of NO<sub>x</sub> (DeNO<sub>x</sub>). It is widely employed in power plants and other industrial settings. Recently, there has been increased interest in adapting this technology to vehicles, especially for heavy-duty diesel engines.<sup>(1)</sup> Urea is typically used as an ammonia source, because it is easily handled and safe to transport.

A number of NH<sub>3</sub>-SCR catalysts have been proposed, including vanadia-loaded titania, copper-loaded zeolites and iron-loaded zeolites. Of these catalysts, Fe/zeolites have been extensively studied, because Fe is a harmless metal and the catalyst has durability toward high temperatures and poisoning.<sup>(2,3)</sup>

NH<sub>3</sub>-SCR generally occurs via three types of

reaction paths, dependent on the NO<sub>2</sub> fraction.<sup>(4,5)</sup> A typical example of this is the reaction between NH<sub>3</sub> and NO, the so-called *standard* SCR:

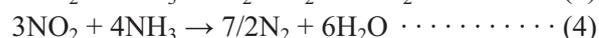
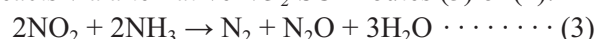


When NO<sub>2</sub> is contained in the feed, an equimolar NO-NO<sub>2</sub> reaction (the so-called *fast* SCR) occurs that is considerably faster than the *standard* SCR reaction (1):



The fast SCR reaction (2) has played a pivotal role in assuring stringent adherence to diesel emission regulations, by using a preoxidation catalyst located upstream of the SCR catalyst in the vehicle. This catalyst converts a fraction of NO to NO<sub>2</sub>, and leads to excellent DeNO<sub>x</sub> activity.

If the NO<sub>2</sub>/NO ratio is larger than 1, then NO<sub>2</sub> also reacts via alternative NO<sub>2</sub> SCR routes (3) or (4).



It is known that NO<sub>2</sub> SCR reactions (3) and (4) are slower than the fast SCR reaction (2) above 200°C.<sup>(4,5)</sup> In addition, nitrous oxide (N<sub>2</sub>O) is detected in a certain temperature range, which is indicative of NO<sub>2</sub>

SCR (3).<sup>(4,5)</sup>

Thus, to attain high DeNO<sub>x</sub> activity, the NO<sub>2</sub>/NO ratio should be fixed to a 1:1 ratio, so that the fast SCR condition can be applied. However, it is difficult to control the ratio using a preoxidation catalyst because the NO<sub>x</sub> concentration, flow rate and temperature can change substantially. In particular, the NO<sub>2</sub> proportion under low temperature conditions will be very low, due to the low activity of the preoxidation catalyst, while at high temperatures the preoxidation catalyst is quite active, and consequently the NO<sub>2</sub> proportion becomes thermodynamically restricted.<sup>(6)</sup> Thus, the NO<sub>2</sub>/NO ratio should vary constantly during engine operation.

Therefore, highly active catalysts should be developed that operate efficiently even under the standard SCR condition, and the reaction mechanisms should be clearly understood to achieve optimal control of the SCR reactions. We have previously investigated the characteristics of Fe/zeolites and reaction behavior of the SCR and SCR-related reactions.<sup>(7-13)</sup> In this report, we present a summary of the results of these studies.

## 2. Development of Fe/zeolite catalysts

### 2.1 Effects of Fe loading method and amount<sup>(7)</sup>

A number of characterization studies of Fe/zeolites have been reported, although the active Fe sites for the SCR reaction are still under debate. The main reason for this continued uncertainty is the coexistence of several Fe species, which prevent identification of the active Fe sites. The distribution of those Fe species is dependent not only on the Fe content, but also on the preparation method. Thus, a large number of preparation methods have been proposed, such as chemical vapor deposition (CVD) of FeCl<sub>3</sub>,<sup>(14)</sup> conventional liquid ion exchange,<sup>(15)</sup> improved liquid ion exchange using Fe complexes<sup>(16)</sup> or iron powder,<sup>(17)</sup> and hydrothermal synthesis.<sup>(18)</sup>

In this study, we prepared a series of Fe/ZSM-5 (Si/Al<sub>2</sub> = 28) catalysts by means of impregnation (Imp), reductive solid-state ion exchange (RSIE) and CVD methods under different levels of Fe loading.<sup>(7)</sup> In order to identify and quantify the active Fe species, characterization was conducted using <sup>57</sup>Fe Mössbauer spectroscopy, Fourier transform infrared (FT-IR) spectroscopy and temperature-programmed desorption (TPD) of NO<sub>2</sub>. For the Imp method, the required amount of Fe was impregnated using an aqueous

Fe(NO<sub>3</sub>)<sub>3</sub> solution and H-ZSM-5 powder. For the RSIE technique, samples prepared using the Imp method were heated at 650°C under reductive conditions (5% H<sub>2</sub>/N<sub>2</sub> flow) for 5 h. For the CVD method, FeCl<sub>3</sub> mixed with dehydrated H-ZSM-5 was sublimed at 650°C for 2.5 h under flowing N<sub>2</sub> and then washed with deionized water. All the samples prepared were finally calcined at 650°C in 20% O<sub>2</sub>/N<sub>2</sub>. The Fe content was determined using inductively coupled plasma-atomic emission spectroscopy (ICP-AES). The samples were denoted as “Method(Fe/Al molar ratio)”, e.g., as CVD(0.78). Catalytic activity tests were carried out under the standard SCR condition using a fixed-bed flow reactor equipped with a gas analyzer.

**Figure 1** shows NO<sub>x</sub> conversions at 250°C as a function of the Fe content. The Imp(0.25–1.00) samples did not exhibit any significant activity, while the RSIE(0.25–1.00) had high activities, which indicates that the reductive high temperature treatment increases the active Fe species. Of all the catalysts, CVD(0.78) exhibited the highest activity; therefore, CVD was determined to be the most effective preparation technique of the three. When Fe/Al > 0.4, the activity decreased according to the sequence CVD > RSIE > Imp. Thus, the generation of active Fe species is more dependent on the preparation method than on the Fe content.

**Figure 2** shows <sup>57</sup>Fe Mössbauer spectra for the Imp(1.00), RSIE(1.00) and CVD(0.78) samples. All the spectra can be deconvoluted into a magnetic sextet

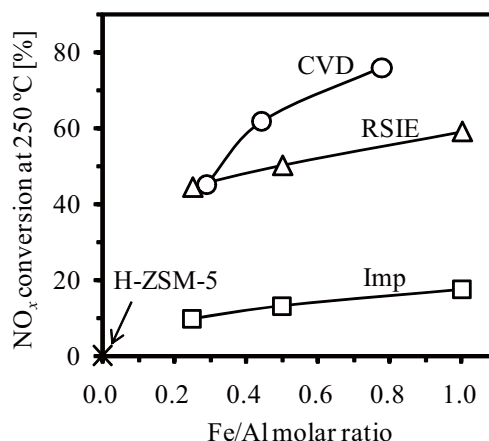


**Fig. 1** NO<sub>x</sub> conversion at 250°C as a function of Fe content. Reaction conditions: 0.1% NO, 0.1% NH<sub>3</sub>, 8% O<sub>2</sub>, 10% CO<sub>2</sub>, 8% H<sub>2</sub>O and balance of N<sub>2</sub>; W/F = 0.20 g/L min.

line and two quadrupole doublet lines. The hyperfine parameters of these spectra are given in **Table 1**, along with the relative integrated intensity of each Fe species. The sextet line is ascribed to large aggregated  $\alpha$ -Fe<sub>2</sub>O<sub>3</sub> particles, and the doublet (I) is probably due to small Fe<sub>2</sub>O<sub>3</sub> particles in the superparamagnetic state (less than 13.5 nm).<sup>(19)</sup> On the other hand, doublet (II) is probably Fe<sup>3+</sup> in a strong, distorted octahedral environment, most likely oxo-Fe<sup>3+</sup> ions at ion-exchanged sites or Fe<sub>x</sub>O<sub>y</sub> oligomers. All the samples

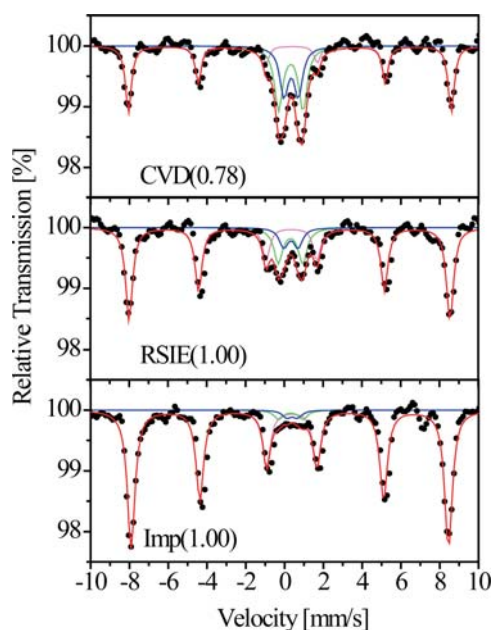


**Fig. 2** <sup>57</sup>Fe Mössbauer spectra at ambient temperature. The curve fitting results are listed in Table 1.

**Table 1** <sup>57</sup>Fe Mössbauer hyperfine parameters and relative intensities of Fe/ZSM-5.

Catalyst	Identification	Isomer shift [mm/s]	Quadrupole splitting [mm/s]	Hyperfine field [kOe]	Relative intensity [%]
Imp(1.00)	Sextet	0.37	-0.1	506	95
	Doublet (I)	0.39	0.55	-	2
	Doublet (II)	0.32	1.26	-	3
RSIE(1.00)	Sextet	0.37	-0.1	515	78
	Doublet (I)	0.34	0.74	-	8
	Doublet (II)	0.32	1.26	-	14
CVD(0.78)	Sextet	0.37	-0.1	515	52
	Doublet (I)	0.34	0.74	-	21
	Doublet (II)	0.32	1.26	-	27

mainly consisted of large  $\alpha$ -Fe<sub>2</sub>O<sub>3</sub> particles in the order Imp(1.00) > RSIE(1.00) > CVD(0.78), which is the same trend observed from X-ray diffraction (XRD) and UV-Vis spectroscopy results (not shown here).<sup>(7)</sup> Thus, the proportion of ion-exchanged Fe and/or oligomeric clusters should be in the converse order. In conclusion, three types of Fe species were mainly present;  $\alpha$ -Fe<sub>2</sub>O<sub>3</sub> particles, Fe<sub>x</sub>O<sub>y</sub> oligomers, and oxo-Fe<sup>3+</sup> at ion-exchanged sites, and these are schematically represented in **Fig. 3**. However, detailed classification of these species is difficult from these Mössbauer spectra. Low temperature measurements under high vacuum conditions are necessary to identify the ion-exchange states and oligomers.

NO<sub>2</sub>-TPD spectra for Fe/ZSM-5 and H-ZSM-5 are presented in **Fig. 4**. Two main peaks are evident around 200 and 350°C; a low-temperature (LT) peak that is essentially independent of Fe content and a high-temperature (HT) peak that is strongly dependent on the preparation method, according to the following order: CVD > RSIE > Imp. The LT peak has been assigned to weakly adsorbed NO<sub>x</sub> in the zeolite channel, and the HT peak to chemisorbed NO<sub>x</sub> bonded to ion-exchanged Fe sites, which was verified by FT-IR peak analysis (T-O-T perturbation peak induced by Fe ion-exchange).<sup>(7,10)</sup>

**Figure 5** shows the relationship between the HT peak amplitude and catalytic activity. NO<sub>x</sub> conversion has an excellent linear correlation with the HT peak amplitude, which suggests that ion-exchanged Fe is the active site for the NH<sub>3</sub>-SCR reaction. Furthermore,

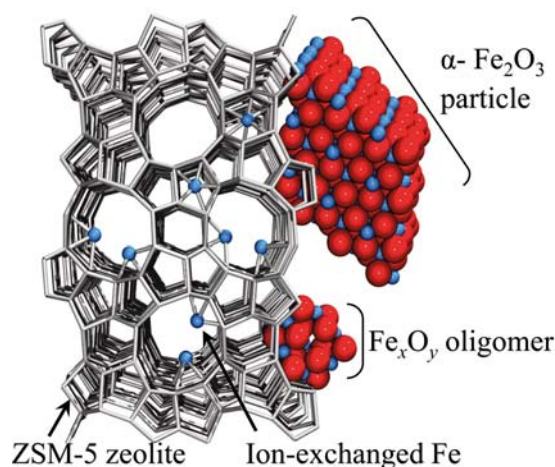


**Fig. 3** Schematic representation of Fe species in Fe/ZSM-5.

NO<sub>2</sub>-TPD enables quantification of the active sites, despite the coexistence of several other Fe species, and it is a powerful technique due to the ease of acquisition and high accuracy compared to other conventional spectroscopic techniques, such as UV-Vis, Mössbauer and FT-IR spectroscopies.

## 2.2 Effects of zeolite structure and Si/Al<sub>2</sub> ratio<sup>(12)</sup>

In the previous section, CVD with high Fe loading to ZSM-5 zeolite was determined to be the most suitable method for producing a high performance NO<sub>x</sub>

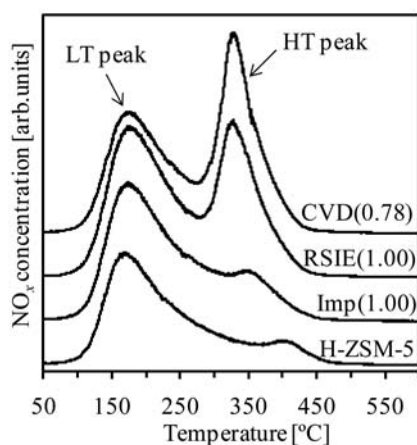


**Fig. 4** NO<sub>2</sub>-TPD spectra of Fe/ZSM-5 and H-ZSM-5. Measurement conditions: heating rate of 10 °C/min under He flow after NO<sub>2</sub> adsorption at 100°C;  $W/F = 4.0$  g/L min.

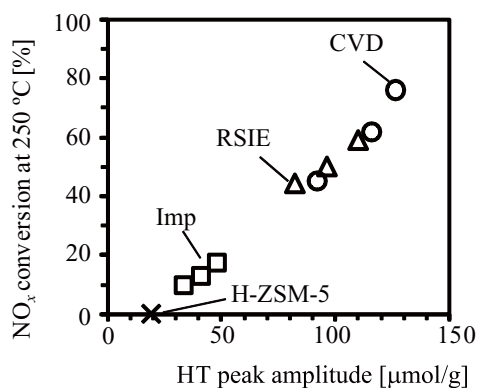


**Fig. 5** NO<sub>x</sub> conversion at 250°C versus the NO<sub>x</sub> amount of the HT peak from NO<sub>2</sub>-TPD over a series of Fe/ZSM-5 catalysts.

SCR catalyst. However, there are relatively few studies that have examined CVD of zeolites with a range of pore structures and Si/Al<sub>2</sub> ratios.<sup>(20,21)</sup> Furthermore, the factors that affect the SCR activity of different types of Fe/zeolites remain unclear. Therefore, in this section, CVD was applied to various zeolites with different pore structures (MFI, BEA, FER, LTL, MOR) and Si/Al<sub>2</sub> ratios (6–240).

H-MFI (ZSM-5, Si/Al<sub>2</sub> = 28, 40, 73, and 90), H-BEA (beta, Si/Al<sub>2</sub> = 27 and 37), H-MOR (mordenite, Si/Al<sub>2</sub> = 20, 30, and 240), H-FER (ferrierite, Si/Al<sub>2</sub> = 18) and H-LTL (L-type, Si/Al<sub>2</sub> = 6) were used as parent zeolites. CVD was conducted at 600°C in a similar way to that described in Section 2.1. The weight ratio of H-zeolite to FeCl<sub>3</sub> was fixed at 5.0, which corresponds to an Fe loading of 6.3 wt%. The Fe/zeolite samples were denoted as “Structure (Si/Al<sub>2</sub> ratio)”, e.g., as MFI(40). Catalytic activity tests were carried out under standard SCR conditions.

**Figure 6** shows NO<sub>x</sub> conversions at 200 and 250°C, where N<sub>2</sub>O was not detected for any of the samples tested. Based on the MFI(40, 73, 90) and MOR(20, 30, 240) data, NO<sub>x</sub> conversion decreased with increasing Si/Al<sub>2</sub> ratio. Furthermore, based on the highest activity from each zeolite structure, NO<sub>x</sub> conversion was ranked as follows: BEA > MFI > FER > LTL > MOR. The inset in Fig. 6 shows NO<sub>x</sub> conversion at 250°C versus the amount of Fe loading determined from ICP-AES; there was no correlation between the activity and

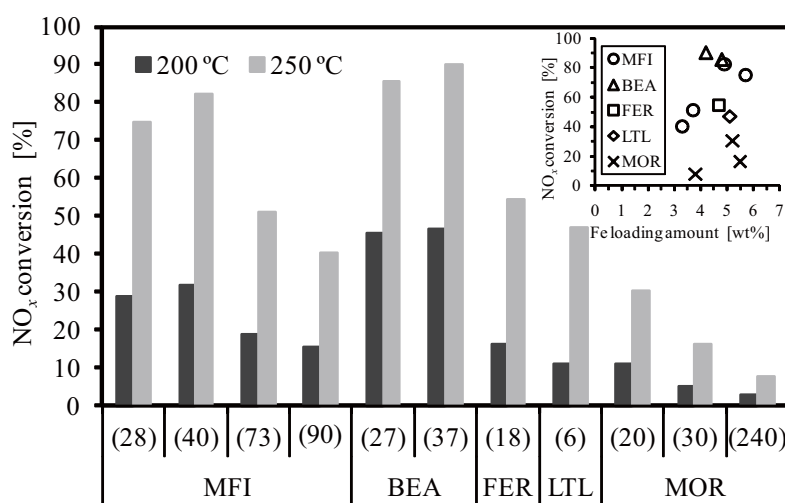


**Fig. 6** NO<sub>x</sub> conversion at 200 and 250°C over Fe/zeolites. Reaction conditions: 0.1% NO, 0.12% NH<sub>3</sub>, 8% O<sub>2</sub>, 10% CO<sub>2</sub>, 8% H<sub>2</sub>O and balance of N<sub>2</sub>;  $W/F = 0.29$  g/L min. Inset: NO<sub>x</sub> conversion at 250°C versus amount of Fe loaded in the catalyst.

Fe content.

To investigate the number of ion-exchanged Fe sites, NO<sub>2</sub>-TPD was conducted for all the Fe/zeolite samples. **Figure 7** shows the correlation between the HT peak magnitude and the NH<sub>3</sub>-SCR activity, which indicates that the SCR performance is dependent on the number of ion-exchanged Fe sites, even for different zeolite structures and Si/Al<sub>2</sub> ratios. Therefore, we can conclude that the major factor that affects SCR performance is the number of active Fe sites. The SCR activity was also correlated with NO oxidation activity measured under NH<sub>3</sub>-free conditions (not shown),<sup>(12)</sup> which suggests that the active Fe sites catalyze the oxidation of NO to NO<sub>2</sub>. This is consistent with the rate-determining step assignment to the formation of NO<sub>2</sub> adspecies,<sup>(8,22)</sup> which is discussed in more detail in Section 3.2.

### 2.3 Stability for hydrothermal aging and sulfur poisoning<sup>(12,13)</sup>

The stability of the Fe/zeolites examined in Section 2.2 against hydrothermal aging and sulfur poisoning was investigated. The condition of hydrothermal aging was 700°C for 5 h under a 3% H<sub>2</sub>O/air flow. The SO<sub>2</sub> poisoning test was conducted using the hydrothermally aged samples with addition of 30 ppm SO<sub>2</sub> to the

reaction gas at 300°C for 20 min. Complete saturation of adsorbed SO<sub>2</sub> was confirmed. Prior to the activity test, all samples were pretreated at 550°C in the reaction gas. **Figure 8** shows a comparison of fresh and aged samples for NO<sub>x</sub> conversion at 250°C. After hydrothermal aging, the NO<sub>x</sub> reduction activity of all Fe/zeolites was lowered. One of the main reasons for the degradation of the Fe/zeolites is the conversion of Al sites from framework positions to extra-framework positions, a process known as dealumination.<sup>(23)</sup> As a result of dealumination, the ion-exchanged Fe sites are lost, which leads to reduced NO<sub>x</sub> conversion. In contrast, SO<sub>2</sub> poisoning caused little change in NO<sub>x</sub> conversion of the Fe/zeolites.

The order of NO<sub>x</sub> conversion for fresh catalysts (BEA > MFI > FER > LTL > MOR) was changed to MFI > BEA > FER > LTL > MOR after hydrothermal aging; the activity of BEA was significantly decreased. The degree of degradation in activity due to the hydrothermal aging differed not only according to differences in the zeolite structure, but also according to the Si/Al<sub>2</sub> ratio. For example, the activity of MFI(73) was much more decreased than that of MFI(40).

In order to quantify the degree of degradation in activity, activity retention rates were estimated based on the ratio of NO<sub>x</sub> conversion for fresh and

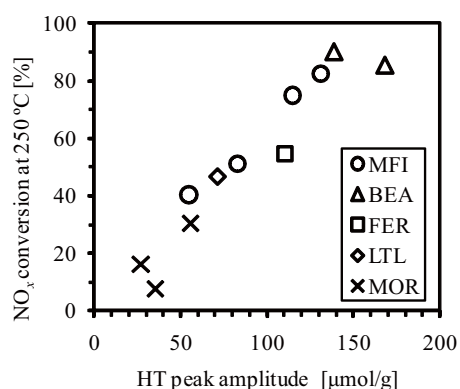


**Fig. 7** NO<sub>x</sub> conversion at 250°C versus HT peak amplitude from NO<sub>2</sub>-TPD over Fe/zeolites. TPD conditions: heating rate of 10 °C/min under N<sub>2</sub> flow after NO<sub>2</sub> adsorption at 100°C; W/F = 0.12 g/L min.

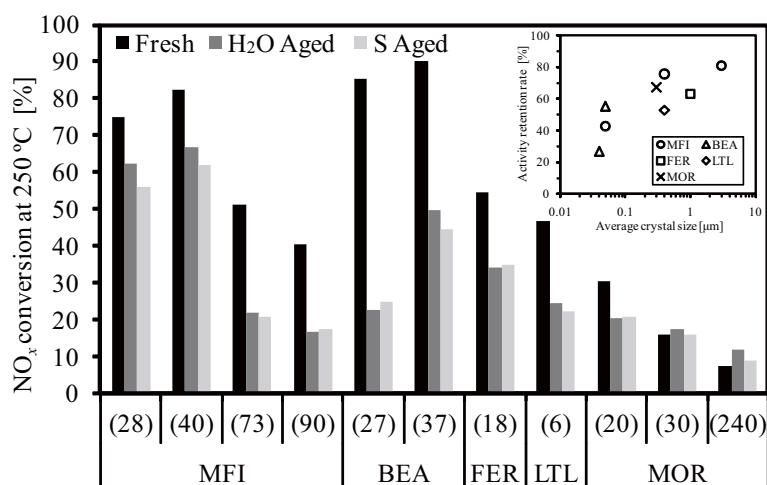


**Fig. 8** Comparison of NO<sub>x</sub> conversion at 250°C for fresh, hydrothermally aged and SO<sub>2</sub> poisoned samples. Hydrothermal aging: 5 h at 700°C in 3% H<sub>2</sub>O/air. SO<sub>2</sub> poisoning: 30 ppm SO<sub>2</sub> at 300°C for hydrothermally aged samples. Inset: Activity retention rate (ratio of NO<sub>x</sub> conversion for hydrothermally aged to fresh catalysts) versus average crystal size of parent H-zeolites.

hydrothermally aged samples. The order of the activity retention rate was not consistent with the order of the SCR activity itself, which suggests that hydrothermal stability is independent of the reaction activity.

The most stable sample was MFI(40) and the least stable sample was BEA(27). Interestingly, the crystal size of MFI(40) was the largest and that of BEA(27) was the smallest of all the samples tested.<sup>(12)</sup> Thus, the relationship between the activity retention rate and crystal size was investigated and the results are shown in the inset of Fig. 8. MOR(30 and 240) were omitted from the comparison, because both would be obtained by dealumination of H-MOR(20). The samples were degraded more when the crystal size was smaller, which indicates that crystal size is an important factor that influences hydrothermal stability.<sup>(24)</sup> However, other factors including pore structure, Al content and the number of Fe exchange sites may have a slight influence on the activity retention rate.

Based on this result, large crystal zeolites have the potential to be used as highly stable catalysts. Thus, if BEA zeolites with larger crystal sizes were used, higher activities could be maintained after hydrothermal aging. Synthesis of larger BEA zeolite crystals has been reported using fluoride media.<sup>(25)</sup>

As another approach to improve the stability, a small addition of rare earth metal can be effective. Sequential ion-exchange of rare earth metal to Fe/BEA was confirmed to improve the hydrothermal stability.<sup>(13)</sup>

### 3. Reaction analysis

#### 3.1 Adsorption and desorption behavior of NO<sub>2</sub><sup>(9,10)</sup>

NO<sub>2</sub>-TPD can be used to estimate the number of ion-exchanged Fe sites, as demonstrated in Sections 2.1 and 2.2. Thus, NO<sub>2</sub> performs a critical function not only in the control of the SCR reactions, but also as a molecular probe to examine the active sites. The NO<sub>2</sub> adsorption step is also an important process in the SCR reactions; however, there have been few reports on NO<sub>2</sub> adsorption/desorption behavior over Fe/zeolites, although such data can provide the most fundamental information required to discuss SCR mechanisms. In this section, the NO<sub>2</sub> adsorption behavior and desorption kinetics are presented.

NO<sub>2</sub> adsorption tests were performed by introducing 0.45% NO<sub>2</sub>/He at 100°C to a reactor equipped with a quadrupole mass spectrometer (QMS). Prior to NO<sub>2</sub> adsorption, the samples were pretreated at 600°C for 30 min in a flow of 5% O<sub>2</sub>/He. The desorption of NO<sub>2</sub> was carried out under He flow at various flow rates and heating rates. The catalyst surface states during NO<sub>2</sub> adsorption were monitored using *in situ* FT-IR. The samples examined were the same as those used in Section 2.1.

**Figure 9(a)** shows the inlet and outlet concentrations of NO and NO<sub>2</sub> with the CVD(0.61) catalyst as a function of time. A large amount of NO evolution with concomitant emission of NO<sub>2</sub> was observed, while

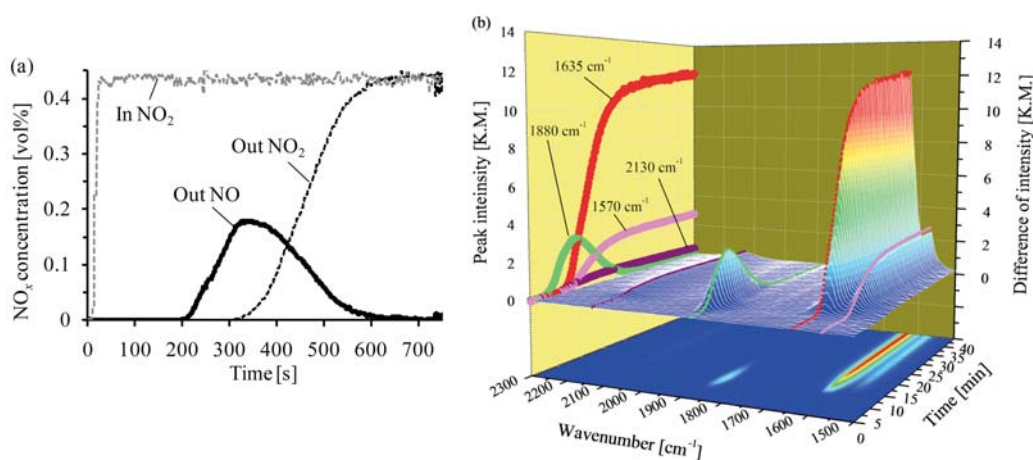


**Fig. 9** (a) NO<sub>x</sub> concentration profile and (b) time-resolved difference FT-IR spectra during NO<sub>2</sub> adsorption over CVD(0.61). Conditions: 0.45% NO<sub>2</sub>/He (W/F = 4.0 g/L min) at 100°C for Fig. 9(a), and 0.1% NO<sub>2</sub>/N<sub>2</sub> (W/F = 0.2 g/L min) at 100°C for Fig. 9(b).

negligible amounts of NO evolution were observed for H-ZSM-5 (not shown).<sup>(10)</sup> Figure 9(b) shows the difference IR spectra within the NO<sub>x</sub> stretching region for CVD(0.61). A band at 1880 cm<sup>-1</sup> appeared temporarily during the first stage of NO<sub>2</sub> adsorption, which then decreased in intensity with the saturation of the other three bands. The three bands at 2130, 1635, and 1570 cm<sup>-1</sup> are assigned to NO<sup>+</sup>, a NO<sub>2</sub> group and a nitrate group, respectively.<sup>(7,10,26)</sup> The band at 1880 cm<sup>-1</sup> was assigned to adsorbed NO species.<sup>(26)</sup> The formation of N<sub>2</sub>O, N<sub>2</sub>O<sub>3</sub> and N<sub>2</sub>O<sub>4</sub> can be ruled out, due to the absence of any additional bands.<sup>(26)</sup> The observation of adsorbed NO agrees well with the NO evolution characteristics.

The ratio of the amount of NO evolution to the HT peak amount from NO<sub>2</sub>-TPD was then calculated for the RSIE and CVD samples. All the ratios were almost half; therefore, it may be expected that one NO molecule evolves from one binuclear site, because the HT peak corresponds to the number of exchanged Fe sites.

Therefore, if combined with the IR results for OH stretching and the zeolite framework vibration regions (not shown),<sup>(10)</sup> we propose the NO evolution process presented in **Fig. 10(a)**. Firstly, Fe–OH species and bridging vacancy sites are available following pretreatment. Secondly, when NO<sub>2</sub> is introduced, NO and bridging oxygen are produced from the decomposition of NO<sub>2</sub>, and then NO is temporarily adsorbed onto the Fe sites. Thirdly, adsorbed NO is then evolved with accompanying substitution of follow-on NO<sub>2</sub>. Figure 10(a) is the key scheme to describe the NO evolution reaction on Fe sites, although it should practically take place only at an upstream position in the catalyst bed.

On the other hand, in the downstream position, where *in situ* FT-IR was monitored, Fig. 10(b)

describes the main process. Firstly, NO generated originally at the upstream position flows downstream and then adsorbs onto the Fe sites. Secondly, follow-on NO<sub>2</sub> is replaced with adsorbed NO and decomposes to produce bridging oxygen by the same step as that in Fig. 10(a).

We finally consider the desorption kinetics of NO<sub>2</sub>. NO<sub>2</sub>-TPD spectra obtained with various flow rates and heating rates revealed that the positions of the LT and HT peaks remained constant, regardless of the flow rate, but shifted to higher temperatures with the heating rates,<sup>(9)</sup> which indicates that desorption is not controlled by an adsorption/desorption equilibrium, i.e., in the no-readsorption limit. Generally, TPD spectra with no-readsorption limit can be expressed as

$$-\frac{d\theta}{dt} = A_d \exp\left(\frac{-E_d}{RT}\right) \theta^n \dots\dots\dots (5)$$

where  $A_d$ ,  $E_d$ ,  $\theta$  and  $n$  are a pre-exponential factor, the desorption energy, surface coverage and desorption order, respectively. A detailed analysis of the TPD spectra with several heating rates can be used to estimate these parameters, which are summarized in **Table 2**. For both peaks, the desorption orders were second-order, which implies that a reverse reaction of dimerization and disproportionation of NO<sub>2</sub> and/or some lateral interaction between NO<sub>2</sub> molecules could be occurring. Furthermore, the NO<sub>2</sub> desorption energy from Fe sites, which is  $E_d$  in the HT peak, was found to be relatively large (138 kJ/mol), which indicates that there are strong interactions between adsorbed NO<sub>x</sub> species and ion-exchanged Fe sites.

### 3.2 Elementary reaction kinetics of standard and fast SCR<sup>(8)</sup>

To understand the transient behavior and reaction

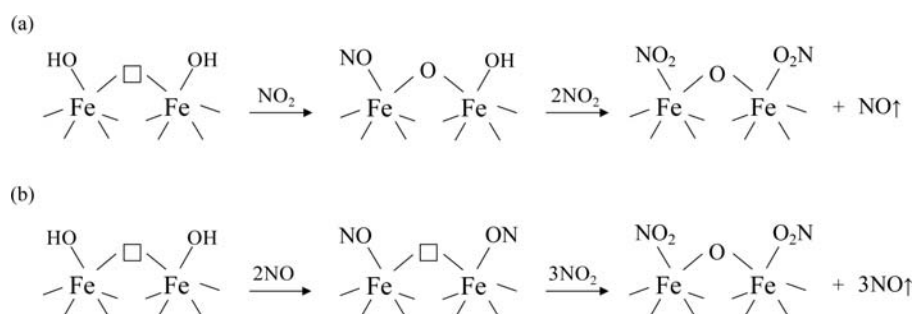


**Fig. 10** Representation of the NO evolution mechanism with NO<sub>2</sub> adsorption over Fe sites at (a) upstream and (b) downstream positions in the catalyst bed.

mechanisms of the standard and fast SCR reactions, periodic NH<sub>3</sub> supply tests and steady-state rate measurements were carried out using a reactor similar to that used in Section 2.1. For the reaction rate measurement, the total gas flow and catalyst weight were controlled to maintain pseudo-differential conditions. Fe/ZSM-5 (Si/Al<sub>2</sub> = 40, Fe/Al = 1.08) prepared by CVD was used as a catalyst.

**Figure 11** shows the outlet NO<sub>x</sub> concentration for the standard and fast SCR conditions. NH<sub>3</sub> was periodically supplied every 500 s. When NH<sub>3</sub> was added to the feed during the standard SCR, the NO<sub>x</sub> concentration quickly decreased to a minimum and then approached a steady-state level. This is due to the heat of NH<sub>3</sub> adsorption plus the heat of the SCR

**Table 2** Estimated desorption parameters of LT and HT peaks in NO<sub>2</sub>-TPD spectra.

	<i>n</i> <sup>a</sup> [-]	<i>A<sub>d</sub></i> <sup>b</sup> [s <sup>-1</sup> ]	<i>E<sub>d</sub></i> <sup>c</sup> [kJ mol <sup>-1</sup> ]
LT peak	≈ 2	10 <sup>5.5±0.2</sup>	67 ± 1
HT peak	≈ 2	10 <sup>9.8±0.3</sup>	138 ± 4

<sup>a</sup> Desorption order.

<sup>b</sup> Pre-exponential factor for desorption.

<sup>c</sup> Activation energy for desorption.

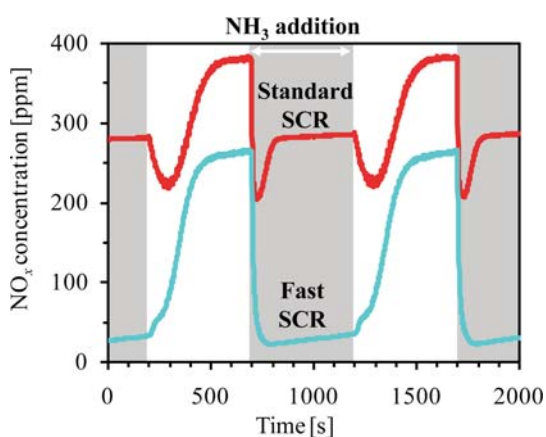


**Fig. 11** Outlet NO<sub>x</sub> concentration during periodic NH<sub>3</sub> supply. Standard SCR: 380 ppm NO, 400 ppm NH<sub>3</sub>, 8% O<sub>2</sub>, 10% CO<sub>2</sub>, 8% H<sub>2</sub>O and balance of N<sub>2</sub>; *W/F* = 0.10 g/L min; *T* = 250°C. Fast SCR: 135 ppm NO, 135 ppm NO<sub>2</sub>, 300 ppm NH<sub>3</sub>, 8% O<sub>2</sub>, 10% CO<sub>2</sub>, 8% H<sub>2</sub>O and balance of N<sub>2</sub>; *W/F* = 0.10 g/L min; *T* = 180°C.

reaction.<sup>(8)</sup> When NH<sub>3</sub> was removed from the feed, the NO<sub>x</sub> concentration again decreased to a minimum and then began to increase, eventually reaching the inlet value. This indicates that the NO<sub>x</sub> reduction rate improved just after NH<sub>3</sub> shutoff. It was confirmed that the N<sub>2</sub> production rate was transiently promoted in the absence of gaseous NH<sub>3</sub>; however, for the fast SCR, no transient NO<sub>x</sub> removal was observed.

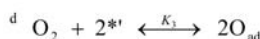
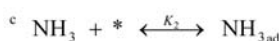
To obtain a deeper understanding of the transient behavior, steady-state rate measurements were performed with variation of the inlet NO<sub>x</sub>, NH<sub>3</sub> and O<sub>2</sub> concentrations. The data was then fitted using elementary reaction models and kinetic parameters were estimated. For the standard SCR, the rate-determining step has been suggested to be NO oxidation between NO<sub>ad</sub> and O<sub>ad</sub> to form NO<sub>2ad</sub>.<sup>(22)</sup> Assuming a Langmuir–Hinshelwood-type mechanism, the overall reaction rate of the standard SCR can be described by the following rate expression:

$$r_1 = k_1 \theta_{NO} \theta_{O_2} = \frac{k_1 K_1 P_{NO} \sqrt{K_3 P_{O_2}}}{(1 + K_1 P_{NO} + K_2 P_{NH_3})(1 + \sqrt{K_3 P_{O_2}})} \dots \dots \dots (6)$$

where  $\theta_i$  and  $P_i$  are the coverage of adsorbate *i* and the partial pressure of gas *i*, respectively. The parameter estimation minimizes the total sum of residual squares between the calculated and experimental reaction rates for each set of isothermal data. The resulting parameter values are summarized in **Table 3**, and the experimental and calculated values for the reaction rate are compared in **Fig. 12**. A good agreement is obtained, which indicates that Eq. (6) is a reasonable and reliable

**Table 3** Optimized kinetic parameters calculated for the standard SCR reaction.

Temperature	<i>k<sub>1</sub></i> <sup>a</sup> [μmol g <sup>-1</sup> s <sup>-1</sup> ]	<i>K<sub>1</sub></i> <sup>b</sup> [atm <sup>-1</sup> ]	<i>K<sub>2</sub></i> <sup>c</sup> [atm <sup>-1</sup> ]	<i>K<sub>3</sub></i> <sup>d</sup> [atm <sup>-1</sup> ]
200 °C	38	106	238	3.2
250 °C	217	33	145	5.7
300 °C	799	15	44	7.4



description, and therefore, the steady-state kinetic analysis confirms that the rate-determining step is the formation of NO<sub>2</sub> adsorbate from NO<sub>ad</sub> and O<sub>ad</sub>. Table 3 shows that the equilibrium constant of NH<sub>3</sub> (K<sub>2</sub>) is larger than that of NO (K<sub>1</sub>), which suggests that the adsorption of NH<sub>3</sub> was much stronger than that of NO. Such strong adsorption inhibits the standard SCR reaction and results in the improvement of NO<sub>x</sub> reduction following NH<sub>3</sub> shutoff in the transient test.

For the fast SCR, when building up a number of related elementary reactions, the fast SCR rate *r<sub>f</sub>* is obtained as a function of only the partial pressures P<sub>*i*</sub>:

$$r_f = \frac{K_4 P_{NO_2} \sqrt{2K_1 K_2 K_3 k_2 k_3 P_{NO} P_{NH_3}}}{1 + K_1 P_{NO} + K_2 P_{NH_3} + K_4 P_{NO_2} \left( 1 + \sqrt{\frac{K_2 K_3 k_2 P_{NH_3}}{2K_1 k_3 P_{NO}}} + \sqrt{\frac{2K_1 K_3 k_3 P_{NO}}{K_2 k_2 P_{NH_3}}} \right)} \dots \dots \dots (7)$$

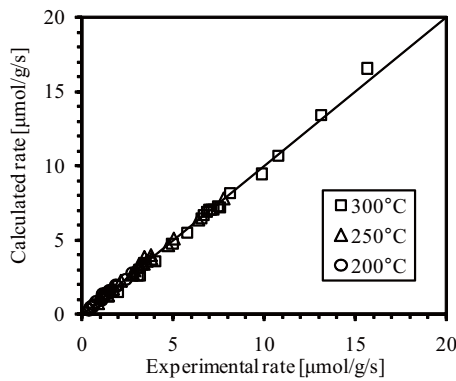


**Fig. 12** Correlation between the experimental and calculated rates for the standard SCR reaction with variation in the inlet gas concentrations. 0.025–0.3% NO, 0.035–0.3% NH<sub>3</sub>, 0.4–19% O<sub>2</sub>, 10% CO<sub>2</sub>, 5% H<sub>2</sub>O and balance of N<sub>2</sub>. W/F = 0.03, 0.06 and 0.07 g/L min at 200, 250 and 300°C, respectively.

Parameter estimations for *k<sub>n</sub>* and *K<sub>n</sub>* were performed, and the results are summarized in **Table 4**. The experimental and calculated values for the reaction rates are compared in **Fig. 13**. From Table 4, *k<sub>3</sub>* is much smaller than *k<sub>2</sub>*, which implies that nitric acid reduction by NO is the rate-determining step. Furthermore, the equilibrium constant of NO<sub>2</sub> (*K<sub>4</sub>*) was larger than that of NH<sub>3</sub> (*K<sub>2</sub>*), which indicates that the adsorption of NO<sub>2</sub> is relatively strong, and this is consistent with the result given in Section 3.1. Thus, it seems plausible that competitive adsorption between NO<sub>2</sub> and NH<sub>3</sub> occurs during the fast SCR, and this must be the main reason for the lack of NO<sub>x</sub> reduction promotion at NH<sub>3</sub> shutoff.

**3.3 Overall reaction analysis of standard, fast and NO<sub>2</sub> SCR<sup>(11)</sup>**

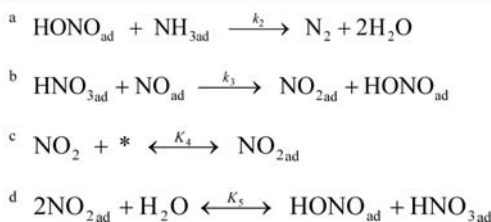
The NO<sub>x</sub> reduction activity over Fe/zeolite when the NO<sub>2</sub>/NO<sub>x</sub> ratio (0–100%) and temperature (150–400°C) are changed in small increments was investigated. The purpose of this study is to elucidate the contribution of standard, fast and NO<sub>2</sub> SCR under conditions where they occur simultaneously, and to establish an overall SCR scheme.

Activity tests were carried out using the same setup described in Section 2.1. Fe/ZSM-5 (Si/Al<sub>2</sub> = 28, Fe/Al = 0.61) prepared by CVD was used as the catalyst. The catalyst was aged at 700°C for 5 h in 3% H<sub>2</sub>O/air.

**Figure 14(a)** shows the degree of NO<sub>x</sub> conversion as a function of both the NO<sub>2</sub>/NO<sub>x</sub> ratio and temperature. NO<sub>x</sub> conversion was strongly dependent on the NO<sub>2</sub>/NO<sub>x</sub> ratio and generally increased with temperature. The highest activity was obtained when the NO<sub>2</sub>/NO<sub>x</sub> ratio was 50%, i.e., under the fast SCR

**Table 4** Optimized kinetic parameters calculated for the fast SCR reaction.

Temperature	<i>k<sub>2</sub><sup>a</sup></i> [μmol g <sup>-1</sup> s <sup>-1</sup> ]	<i>k<sub>3</sub><sup>b</sup></i> [μmol g <sup>-1</sup> s <sup>-1</sup> ]	<i>K<sub>1</sub></i> [atm <sup>-1</sup> ]	<i>K<sub>2</sub></i> [atm <sup>-1</sup> ]	<i>K<sub>4</sub><sup>c</sup></i> [atm <sup>-1</sup> ]	<i>K<sub>5</sub><sup>d</sup></i> [no unit]
195 °C	2.3 × 10 <sup>6</sup>	9.5 × 10 <sup>2</sup>	290	539	656	2.5 × 10 <sup>-4</sup>
250 °C	7.3 × 10 <sup>6</sup>	6.9 × 10 <sup>3</sup>	161	199	468	3.4 × 10 <sup>-5</sup>



conditions. In addition,  $\text{NO}_x$  conversion for the standard SCR was less than that for  $\text{NO}_2$  SCR. Therefore, the activities for the SCR reactions are ranked in terms of  $\text{NO}_x$  conversion as follows: fast SCR >  $\text{NO}_2$  SCR > standard SCR. Figure 14(b) shows the concentration of  $\text{N}_2\text{O}$  produced. The amount of  $\text{N}_2\text{O}$  observed when  $\text{NO}_2/\text{NO}_x < 50\%$  was negligible, whereas  $\text{N}_2\text{O}$  was increased when  $\text{NO}_2/\text{NO}_x > 50\%$ . Therefore,  $\text{N}_2\text{O}$  production seems to be responsible for  $\text{NO}_2$  SCR. Furthermore, the  $\text{N}_2\text{O}$  concentration was highest at around 250–300°C, which suggests that  $\text{N}_2\text{O}$  production is dependent on the temperature.

When the contribution of  $\text{N}_2\text{O}$  production was eliminated from the  $\text{NO}_x$  conversion, i.e., the  $\text{NO}_x$

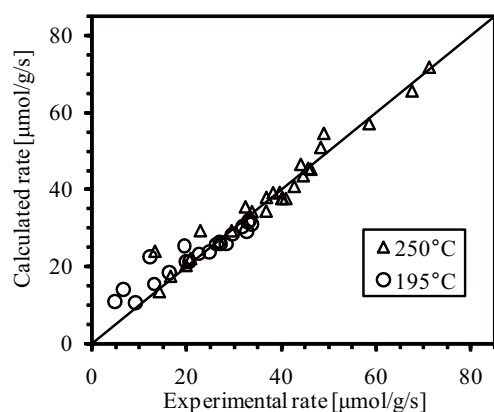


**Fig. 13** Correlation between the experimental and calculated rates for the fast SCR reaction with variation in the inlet gas concentrations. 0.014–0.15%  $\text{NO}$ , 0.015–0.13%  $\text{NO}_2$ , 0.023–0.28%  $\text{NH}_3$ , 0.4–19%  $\text{O}_2$ , 10%  $\text{CO}_2$ , 5%  $\text{H}_2\text{O}$  and balance of  $\text{N}_2$ .  $W/F = 0.012$  g/L min.

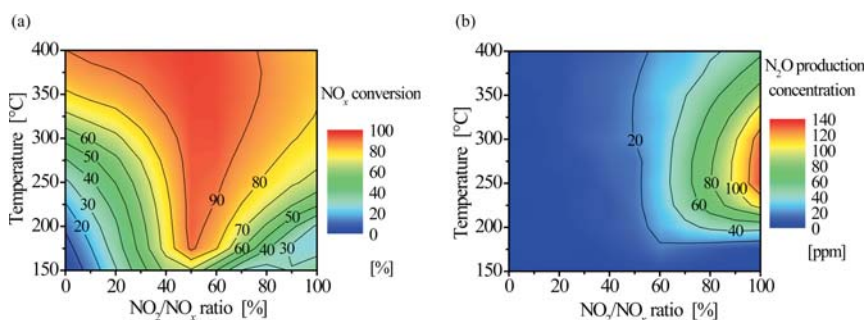


**Fig. 14** Map of (a)  $\text{NO}_x$  conversion and (b)  $\text{N}_2\text{O}$  production versus  $\text{NO}_2/\text{NO}_x$  ratio and temperature.  $\Delta(\text{NO}_2/\text{NO}_x \text{ ratio}) = 25\%$ ;  $\Delta T = 25^\circ\text{C}$ ; Feed = 380 ppm  $\text{NO}_x$  ( $\text{NO} + \text{NO}_2$ ), 400 ppm  $\text{NH}_3$ , 8%  $\text{O}_2$ , 10%  $\text{CO}_2$ , 8%  $\text{H}_2\text{O}$  and balance of  $\text{N}_2$ ;  $W/F = 0.1$  g/L min.

conversion was estimated with exclusion of the  $\text{N}_2\text{O}$  production, the activity ranking for the three reactions was changed to fast SCR > standard SCR >  $\text{NO}_2$  SCR.<sup>(11)</sup> This result strongly indicates that the influence of  $\text{N}_2\text{O}$  production during  $\text{NO}_x$  conversion cannot be ignored, especially in the higher  $\text{NO}_2/\text{NO}_x$  region. Furthermore, when the fast SCR conversion was subtracted from the total  $\text{NO}_x$  conversion, the obtained “apparent” conversions were independent of the  $\text{NO}_2/\text{NO}_x$  ratio.<sup>(11)</sup> Therefore, the standard and  $\text{NO}_2$  SCR reactions proceeded once the fast SCR reaction was completed.

In order to understand the low temperature behavior of the three SCR reactions, the  $\text{NO}_x$  conversion reactions were repeated with smaller temperature steps below 200°C. Figure 15 shows the  $\text{NO}_x$  conversions for the three SCR reactions and the  $\text{N}_2\text{O}$  selectivity of the  $\text{NO}_2$  SCR reaction. Interestingly, the temperature dependence of each reaction was quite different. The standard SCR conversion was gradually lowered with decreasing temperature, while the fast SCR conversion dropped suddenly at around 175°C. However, the  $\text{NO}_2$  SCR conversion went through a minimum at around 185°C and then began to increase with decreasing temperature. The  $\text{N}_2\text{O}$  selectivity of the  $\text{NO}_2$  SCR reaction began to increase with temperature above 175°C, and then reached ca. 50% at 225°C. This corresponds to the overall stoichiometry of reaction (3). It should be noted that  $\text{N}_2\text{O}$  was not detected below 175°C, despite the increase in  $\text{NO}_x$  conversion for  $\text{NO}_2$  SCR with the decrease in temperature. This infers that

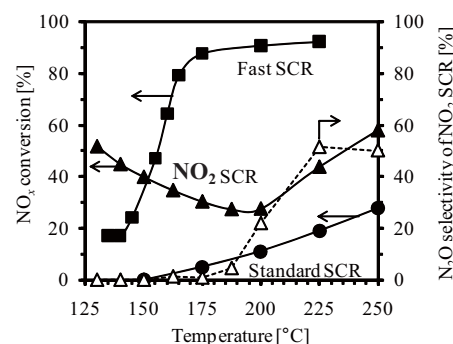


**Fig. 15**  $\text{NO}_x$  conversion for the standard ( $\text{NO}_2/\text{NO}_x = 0\%$ ), fast ( $\text{NO}_2/\text{NO}_x = 50\%$ ) and  $\text{NO}_2$  ( $\text{NO}_2/\text{NO}_x = 100\%$ ) SCR reaction, and  $\text{N}_2\text{O}$  selectivity of the  $\text{NO}_2$  SCR. Reaction conditions are the same as those given in Fig. 14.

some new reaction path may be available below 175°C.

**Figure 16** shows a schematic summary of the SCR scheme. The rate-determining step for each SCR reaction is depicted as a circle. A common reaction in each SCR is the formation of a surface ammonium nitrate species from adsorbed  $\text{NO}_2$ . The reason why the fast SCR has the highest activity among the three SCR reactions is that the rate-determining step for the fast SCR proceeds at the fastest rate. However, a drastic decline in fast SCR conversion was observed at around 175°C (Fig. 15), which is near the melting point of ammonium nitrate. Thus, the abrupt decrease in the fast SCR rate is responsible for the inhibition of the rate-determining step by the formation of stable ammonium nitrate. In contrast,  $\text{NO}_2$  SCR conversion increased with a decrease in the temperature below 185°C. It is considered that this negative temperature dependence of the  $\text{NO}_x$  conversion is attributed to the promotion of ammonium nitrate desorption, which is inhibited by nitric acid (or nitrate ion) adspecies when the temperature increases.

#### 4. Conclusions

This article presented the development and characterization of Fe/zeolite catalysts for  $\text{NH}_3$ -SCR of  $\text{NO}_x$ , and analysis of the reaction kinetics for SCR using a Fe/ZSM-5 catalyst. The reaction activity was dependent on the Fe loading (preparation and Fe content) and the pore structure and Si/Al<sub>2</sub> ratio of the

zeolite species. A major factor that affected the SCR performance was the number of active Fe sites. In addition, active ion-exchanged Fe sites were accurately quantified using  $\text{NO}_2$ -TPD. Therefore, this investigation provided very important information and techniques required for the development of Fe/zeolite catalysts.

Analysis of the reaction kinetics revealed that NO evolution following  $\text{NO}_2$  adsorption occurs over binuclear Fe sites, and the adsorption strength of  $\text{NO}_2$  onto the Fe sites was relatively large (138 kJ/mol). The standard SCR reaction was transiently promoted in the absence of gaseous  $\text{NH}_3$ , because  $\text{NH}_3$  inhibited the rate-determining step. However, for the fast SCR, no promotion behavior was observed, due to the competitive adsorption of  $\text{NO}_2$  and  $\text{NH}_3$ . The overall SCR scheme was presented as a function of the  $\text{NO}_2/\text{NO}_x$  ratio and temperature, from which a comprehensive understanding of the SCR mechanisms were obtained, and thus establish the general chemistry of SCR reactions for the practical development of catalysts in diesel engines.

#### References

- (1) Johnson, T. V., *Int. J. Engine Res.*, Vol.10 (2009), pp.275-285.
- (2) Long, R. Q. and Yang, R. T., *J. Am. Chem. Soc.*, Vol.121 (1999), pp.5595-5596.
- (3) Ma, A. -Z. and Grünert, W., *Chem. Commun.* (1999), pp.71-72.
- (4) Koebel, M., Madia, G. and Elsener, M., *Catal. Today*, Vol.73 (2002), pp.239-247.
- (5) Grossale, A., Nova, I. and Tronconi, E., *Catal. Today*, Vol.136 (2008), pp.18-27.
- (6) Olsson, L., Westerberg, B., Persson, H., Fridell, E., Skoglundh, M. and Andersson, B., *J. Phys. Chem. B*, Vol.103 (1999), pp.10433-10439.
- (7) Iwasaki, M., Yamazaki, K., Banno, K. and Shinjoh, H., *J. Catal.*, Vol.260 (2008), pp.205-216.
- (8) Iwasaki, M., Yamazaki, K. and Shinjoh, H., *Appl. Catal. A: Gen.*, Vol.366 (2009), pp.84-92.
- (9) Iwasaki, M. and Shinjoh, H., *Phys. Chem. Chem. Phys.*, Vol.12 (2010), pp.2365-2372.
- (10) Iwasaki, M. and Shinjoh, H., *J. Catal.*, Vol.273 (2010), pp.29-38.
- (11) Iwasaki, M. and Shinjoh, H., *Appl. Catal. A: Gen.*, Vol.390 (2010), pp.71-77.
- (12) Iwasaki, M., Yamazaki, K. and Shinjoh, H., *Appl. Catal. B: Environ.*, Vol.102 (2011), pp.302-309.
- (13) Iwasaki, M. and Shinjoh, H., *Chem. Commun.*, Vol.47 (2011), pp.3966-3968.
- (14) Chen, H. -Y. and Sachtler, W. M. H., *Catal. Today*, Vol.42 (1998), pp.73-83.

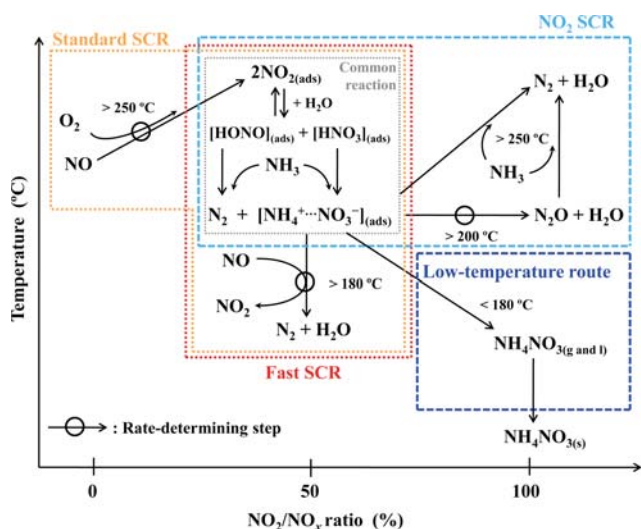


**Fig. 16** Proposed overall SCR scheme as a function of the  $\text{NO}_2/\text{NO}_x$  ratio and temperature.

- (15) Long, R. Q. and Yang, R. T., *J. Catal.*, Vol.194 (2000), pp.80-90.
- (16) Delahay, G., Valade, D., Guzmán-Vargas, A. and Coq, B., *Appl. Catal. B: Environ.*, Vol.55 (2005), pp.149-155.
- (17) Long, R. Q. and Yang, R. T., *Catal. Lett.*, Vol.74 (2001), pp.201-205.
- (18) Ribera, A., Arends, I. W. C. E., de Vries, S., Pérez-Ramírez, J. and Sheldon, R. A., *J. Catal.*, Vol.195 (2000), pp.287-297.
- (19) Kündig, W. and Bömmel, H., *Phys. Rev.*, Vol.142 (1966), pp.327-333.
- (20) Chen, H. -Y., Wang, X. and Sachtler, W. M. H., *Appl. Catal. A: Gen.*, Vol.194-195 (2000), pp.159-168.
- (21) Qi, G., Gatt, J. E. and Yang, R. T., *J. Catal.*, Vol.226 (2004), pp.120-128.
- (22) Long, R. Q. and Yang, R. T., *J. Catal.*, Vol.207 (2002), pp.224-231.
- (23) Kröcher, O., Devadas, M., Elsener, M., Wokaun, A., Söger, N., Pfeifer, M., Demel, Y. and Musmann, L., *Appl. Catal. B: Environ.*, Vol.66 (2006), pp.208-216.
- (24) Panpranot, J., Toophorm, U. and Praserthdam, P., *J. Porous Mater.*, Vol.12 (2005), pp.293-299.
- (25) Simon-Masseron, A., Marques, J. P., Lopes, J. M., Ribeiro, F. R., Gener, I. and Guisnet, M., *Appl. Catal. A: Gen.*, Vol.316 (2007), pp.75-82.
- (26) Gao, Z. -X., Sun, Q. and Sachtler, W. M. H., *Appl. Catal. B Environ.*, Vol.33 (2001), pp.9-23.

Figs. 9(b) and 10

Reprinted from *J. Catal.*, Vol.273 (2010), pp.29-38, Iwasaki, M. and Shinjoh, H., NO evolution reaction with NO<sub>2</sub> adsorption over Fe/ZSM-5: In situ FT-IR observation and relationships with Fe sites, Copyright 2010, with permission from Elsevier.

Figs. 12 and 13

Reprinted from *Appl. Catal. A: Gen.*, Vol.366 (2009), pp.84-92, Iwasaki, M., Yamazaki, K. and Shinjoh, H., Transient reaction analysis and steady-state kinetic study of selective catalytic reduction of NO and NO + NO<sub>2</sub> by NH<sub>3</sub> over Fe/ZSM-5, Copyright 2009, with permission from Elsevier.

Figs. 14 and 16

Reprinted from *Appl. Catal. A: Gen.*, Vol.390 (2010), pp.71-77, Iwasaki, M. and Shinjoh, H., A comparative study of "standard", "fast" and "NO<sub>2</sub>" SCR reactions over Fe/zeolite catalyst, Copyright 2010, with permission from Elsevier.

---

#### Masaoki Iwasaki

Research Field :

- Automotive catalyst

Academic Societies :

- Chemical Society of Japan

- Catalysis Society of Japan

